ANNALI DI GEOFISICA, VOL. XXXVII, N. 6, December 1994

# From tomographic images to fault heterogeneities

**Claudio Chiarabba and Alessandro Amato**
*Istituto Nazionale di Geofisica, Roma, Italy*

**Abstract**
Local Earthquake Tomography (LET) is a useful tool for imaging lateral heterogeneities in the upper crust. The pattern of *P*- and *S*-wave velocity anomalies, in relation to the seismicity distribution along active fault zones, can shed light on the existence of discrete seismogenic patches. Recent tomographic studies in well monitored seismic areas have shown that the regions with large seismic moment release generally correspond to high velocity zones (HVZ's). In this paper, we discuss the relationship between the seismogenic behavior of faults and the velocity structure of fault zones as inferred from seismic tomography. First, we review some recent tomographic studies in active strike-slip faults. We show examples from different segments of the San Andreas fault system (Parkfield, Loma Prieta), where detailed studies have been carried out in recent years. We also show two applications of LET to thrust faults (Coalinga, Friuli). Then, we focus on the Irpinia normal fault zone (South-Central Italy), where a $M_S = 6.9$ earthquake occurred in 1980 and many thousands of aftershock travel time data are available. We find that earthquake hypocenters concentrate in HVZ's, whereas low velocity zones (LVZ's) appear to be relatively aseismic. The main HVZ's along which the mainshock rupture has propagated may correspond to velocity weakening fault regions, whereas the LVZ's are probably related to weak materials undergoing stable slip (velocity strengthening). A correlation exists between this HVZ and the area with larger coseismic slip along the fault, according to both surface evidence (a fault scarp as high as 1 m) and strong ground motion waveform modeling. Smaller wave-length, low-velocity anomalies detected along the fault may be the expression of velocity strengthening sections, where aseismic slip occurs. According to our results, the rupture at the nucleation depth (~ 10-12 km) is continuous for the whole fault length (~ 30 km), whereas at shallow depth, different fault segments are activated due to lateral heterogeneities in the sedimentary cover. This finding confirms that the rupture process is controlled by lithologic and structural discontinuities in the upper crust, and emphasizes the contribution that LET can make to the study of fault mechanics.

**Key words** *seismic tomography – fault structure – seismogenic behavior*

## 1. Introduction

The aim of this paper is to discuss the contribution of local earthquake tomography (LET) to the understanding of earthquake source mechanics. We are motivated by recent hypotheses regarding the control of rheological heterogeneities on faulting behavior (Boatwright and Cocco, 1994, and references therein), and the heterogeneous distribution of frictional properties along fault zones. If the occurrence of different scales of seismic strain release (as large events, aftershocks, microseismicity) depends on fault rheology and material properties, we can predict the seismogenic behavior of a fault from crustal velocity images. Large crustal earthquakes (*i.e.*, $M \geq 6.5$) are generated by faults with dimensions of some tens of kilometers, a size that can be well imaged by LET, which has the resolution of a few kilometers (typically, 2-5 km).

The identification of faults and tectonic processes has been a central goal of tomographic studies in several seismic areas (*e.g.*, Eberhart-

Phillips, 1993, and references therein). In this paper, we review some examples and conclusions achieved by these studies, emphasizing the relation between velocity anomalies, slipped fault patches during large events, and cluster of aftershocks. We also use the tomograms to infer the presence of different fault patches (and fault heterogeneities) characterized by different frictional stability properties that control different types of seismic release. The main perception derived from most tomographic studies is that *high* and *low* velocity zones represent the expression of fault segments characterized by *strong* and *weak* behavior (Zhao and Kanamori, 1992; Foxall *et al.*, 1993).

Sharp velocity contrasts are often observed across major faults and are generally interpreted as lithological discontinuities (Michelini and McEvilly, 1991; Amato *et al.*, 1992; Eberhart-Phillips and Michael, 1993). A strong gradient maps the location of the fault at depth, where aftershocks are clustered. However, we note that the presence of velocity gradients rather than discontinuities in a tomographic image may be linked to the model parameterization and to the definition of velocities within the volume (linear interpolation between nodes of a three-dimensional grid), or to smoothing constraints applied to resolve the inverse problem. Thus, the velocity gradients commonly modeled may be a shadow of stronger velocity contrasts across the faults.

Along the fault, high velocities commonly delineate the extent of regions with brittle behavior, in which most of the coseismic slip concentrates. Conversely, low velocities characterize areas with deficit of coseismic slip and aftershocks (Michael and Eberhart-Phillips, 1991; Amato *et al.*, 1992; Foxall *et al.*, 1993). We relate the brittle HVZ's to fault segments characterized by a velocity weakening mechanism, whereas in the LVZ's a velocity strengthening behavior is more likely.

In addition, the fluid saturation and pore pressure in the rocks lead to variations in seismic velocities. This phenomenon affects *P*- and *S*-wave velocity differently. Thus, the presence of fluids, which play a fundamental role in rock mechanics and rheology (Byerlee, 1990; Scholz, 1990; Rice, 1992; Hill, 1993; Chester *et al.*, 1993, among many others), can be evinced by tomographic studies that include the *S*-wave data. The large uncertainty associated with *S*-wave arrival times and the inversion for the *S*-wave model, however, is still a serious limit for seismic tomography. Thus, we are still not able to determine if the variation of the friction coefficient or of the pore pressure is responsible for the shear resistance variation.

After the review, we present our tomographic study of the Irpinia 1980 normal faulting earthquake. Our aim is to develop a synoptic representation of the seismogenic zone, including all the available observations together with the tomograms. We are mainly interested in the relation between velocity anomalies and earthquake characteristics, rather than a particular model for that earthquake. We select the Irpinia event because several aftershock arrival times are available and because the robustness of the 3-D inversion has been established (Amato *et al.* 1992). Furthermore, Irpinia is one of the few normal faulting events in the world for which many kinds of geologic and seismologic data are available.

## 2. Local Earthquake Tomography (LET), where, why, and how

The primary benefit of using LET in earthquake source zones is the possibility of modeling an area with seismological significance. Because larger events often occur with evidence of «characteristic behavior» along preexisting structures (Allen, 1981; Schwartz and Coppersmith, 1984), refined images of the crustal structure in these areas seem to be a powerful tool for delineating their seismic potential. Our aim is to image the local heterogeneities along the fault that may control rupture nucleation and stopping. The apparent circularity of our logic, in needing earthquake arrival times for tomography, and then identifying the internal structure of seismogenic zones that already experienced a large event, is exceeded considering that tomographic experiments can be executed in seismic areas largely

before earthquakes (with artificial sources or background seismicity, for instance).

Another advantage of LET is that in seismic areas we can use numerous «low-cost» crossing raypaths due to the large number of aftershocks usually recorded after large events. The target volume is well sampled by the rays close to the fault, allowing us to reach a fine definition of heterogeneities. The high-frequency characteristic of aftershock waveforms at LET distances (generally $\geq$ 5 Hz) ensures a high resolution capability of the data. The resolution of modeled anomalies is mainly limited by the station spacing, rather than the signal frequency content. Generally, the maximum achievable resolution is of 1-2 km, although the ray geometry and the inversion procedure smear the velocity computation over larger volumes.

The goal of LET in seismic areas is the definition of crustal velocity structure of fault zones. Identifying the deep geologic structure is fundamental to characterizing tectonic processes, the geometry and extent of faults. This applies particularly to thrust events, where the faults often do not break the surface (blind thrusts) and are therefore difficult to investigate (Eberhart-Phillips, 1990; Stein and King, 1984; Stein, 1993).

Two major questions arise: *can different fault segments (such as asperities or barriers) be resolved via LET*?, and *is the rheologic behavior of rocks directly related to seismic velocity*? We believe that lithological heterogeneities yield variations in the frictional properties in fault zones and may have a strong influence on fault slip and earthquake dynamics (Foxall *et al.*, 1993; J. Boatwright personal communication, 1994). These heterogeneities can be recovered with LET (Eberhart-Phillips and Michael, 1993; Amato *et al.*, 1992), because they are closely associated with seismic velocity variation in the uppermost crust. Material inhomogeneities behave like dynamic heterogeneities during the seismic stress release. Therefore, we can try to infer the rheologic behavior from material property variations (seismic velocity in our case).

LET is based on the inversion of *P*- and *S*-wave arrival times (Aki and Lee, 1976). The basic idea is that differences in ray-path travel times within a region are somehow related to seismic wave velocities inside the travelled volume. Thus, *P*- and *S*-wave arrival times at an array of stations contain an (unfortunately unknown) amount of information on the velocity structure (Thurber, 1983). More generally, the arrival times are coupled to both earthquake hypocentral locations and velocity model (Thurber, 1992). Their partition, obviously not known *a priori*, needs to be taken into account while inverting the data. For this reason we prefer the tomographic approach of «simultaneous inversion» (see Thurber, 1993, and references therein), with respect to the «tomography in sensu strictu» where the hypocenters are kept fixed, and only the model velocity parameters are inverted (Lees and Malin, 1990, and references therein). Furthermore, simultaneous inversion remains a highly non-linear problem, with an intrinsic trade-off between earthquake location and velocity parameters computation. This trade-off is resolved separating the medium parameters from the hypocentral ones (Pavlis and Booker, 1980). After obtaining earthquake locations, the technique computes the velocities averaging the values over a (more or less localized) volume of the medium. Velocities are defined with a discrete number of points (in our case nodes of a three-dimensional grid).

The non-linear inversion is solved minimizing a measure of the data misfit – the residuals – with an iterative scheme. In each iteration a starting guess of model parameters is perturbed, and linearity is justified when applying small perturbations. Thus, choosing the starting model becomes fundamental to the convergence of the problem toward the global minimum.

The travel-time residual is defined as the difference of the observed arrival time for an event $j$ at a station $i$ as

$$r_{ij} = t_{ij}^{obs} - t_{ij}^{cal} = \sum_{k=1}^{4} \frac{\partial T_{ij}}{\partial x_k} \Delta x_k + \sum_{l=1}^{L} \frac{\partial T_{ij}}{\partial m_l} \Delta m_l \,, \qquad (2.1)$$

where $m_l$ are the $L$ parameters of the velocity model, $\frac{\partial T_{ij}}{\partial x_k}$ are the variations of $T$ with respect to hypocentral coordinates and origin time, $\frac{\partial T_{ij}}{\partial m_l}$ are the variations of $T$ with respect to the model parameters, and $\Delta x_k$, $\Delta m_l$ are the unknown parameters. The computation of the model parameters is performed using a damped-least-squares inversion

$$\Delta m = ((\boldsymbol{M})^T \boldsymbol{M} + \theta^2 \boldsymbol{I})^{-1} (\boldsymbol{M})^T r' \qquad (2.2)$$

where $r'$ is the vector of residuals, $\boldsymbol{M}$ is the resolving kernel, $\theta^2$ is a damping parameter added to the diagonal of the medium matrix to reduce the large velocity perturbations that can occur for singularity in $\boldsymbol{M}$ (a similar damping is imposed on hypocentral variables after parameter separation).

Several LET techniques have been developed, mainly differing in the treatment of model parameterization, ray-tracing, hypocenter-velocity parameters coupling, inversion technique, evaluation of model resolution (Thurber, 1993; Eberhart-Phillips, 1993, and references therein).

## 3. Tomographic applications in fault zones

LET has provided three-dimensional structure images of several fault systems at seismogenic depths. Here, we present the results obtained by different authors for some significant

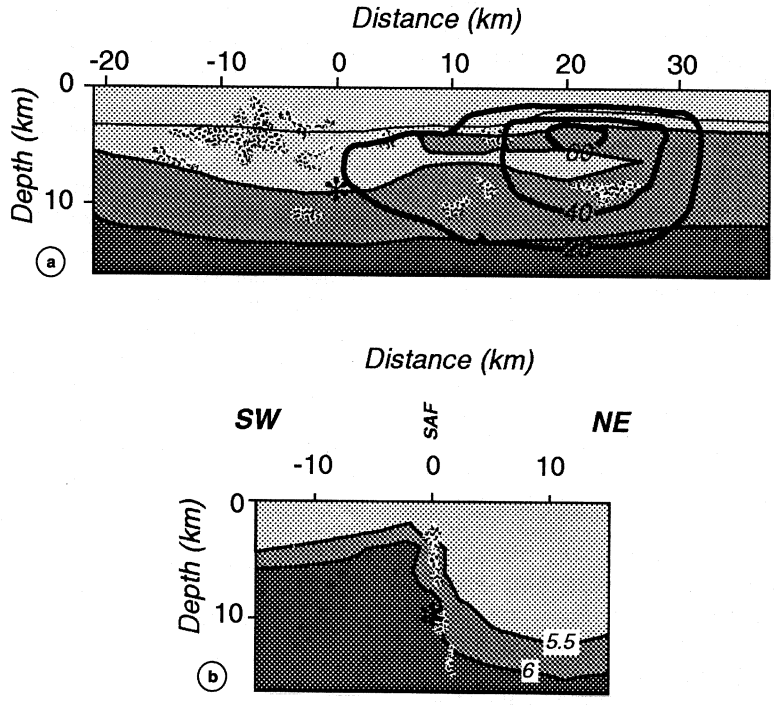


**Fig. 1a,b.** Parkfield: $V_p$ images (a) along and (b) across the fault (redrawn after Michael and Eberhart-Phillips, 1991). Star indicates the 1966 mainshock hypocenter, dotted areas are clusters of background seismicity, solid lines delineate coseismic slip distribution according to Segall and Harris (1987).

fault structures, in strike-slip and thrust faults. Then, we describe in detail the application of LET to the Irpinia region, where a $M_S$ 6.9 earthquake occurred in 1980, in order to show the relation between velocity structure of the fault zone, nucleation, propagation and arrest of the main rupture, and the aftershock distribution.

### 3.1. *Strike-slip faults*

Because many active faults that have produced large events in recent years occurred with strike-slip mechanisms, we start our review from this kind of faults. One of the best known such faults is the *Parkfield* segment of the San Andreas Fault (SAF), which has repeatedly produced earthquakes of $M \sim 6$ (Bakun and McEvilly, 1984). Here, the SAF is imaged as a sharp horizontal $V_p$ gradient between higher velocity on the south-western side and lower velocities on the north-eastern side (Lees and Malin, 1990; Michelini and McEvilly, 1991; Eberhart-Phillips and Michael, 1993). Below the surface fault trace, the sharp gradient maps the fault extension at seismogenic depth (see fig. 1a,b). Along the fault, background seismicity, shown on the 3-D tomograms (fig. 1a,b), marks the boundary of the high velocity. Coseismic slip along the fault (Segall and Harris, 1987) is dominant in the HVZ, whereas it decreases toward NW in the low velocity creeping section of the fault. Michael and Eberhart-Phillips (1991) and Eberhart-Phillips and Michael (1993) suggest that a relation exists between high velocity and »increasing ability of the rocks to store strain energy and release it as brittle failure».

A second extensively studied area is the *Loma Prieta* section of the SAF (Dietz and Ellsworth, 1990; Oppenheimer, 1990; Segall and Lisowsky, 1990; Beroza, 1991). A HVZ trending SE-NW has been imaged by Michael and Eberhart-Phillips (1991) and Foxall *et al.* (1993) from 2 to 8 km depth beneath the SAF trace. Although several explanations have been proposed for the origin of this body (see Foxall *et al.*, 1993), we are mainly interested in the concidence of the HVZ and the area ruptured during the mainshock (Lisowski *et al.*, 1990). Across the fault, seismicity is associated with the sharp velocity contrast (fig. 2a,b), and material with $V_p \geq 6$ km/s experienced brittle failure. Foxall *et al.* (1993) propose that the high velocity body is responsible for the stable to unstable slip transition, due to variations of frictional properties within the fault.

### 3.2. *Thrust faults*

Local earthquake tomography applied to areas of crustal convergence is an important tool to investigate buried folds and blind thrusts (Eberhart-Phillips, 1993; Roecker, 1993). The combined interpretation of seismicity, fault plane solutions, and velocity anomalies at depth allows one to recover the geometrical style of deformation of these complex geologic structures. Here we describe two examples of blind thrust faults that generated strong ($M \sim 6.5$) earthquakes and a diffuse distribution of aftershocks. The two regions are at Coalinga, California (Eberhart-Phillips, 1989, 1990), and in Friuli, Italy (Amato *et al.*, 1990).

The Coalinga earthquake sequence occurred in 1983 and has been extensively studied by Eberhart-Phillips (1989, 1990), who pointed out the existence of a suite of southwest-dipping blind thrusts at the base of a fold. The fold is well imaged at depth by LET and has its surface expression in the Coalinga anticline (fig. 3). The nearly horizontal thrust faults, which are imaged as LVZ, uplift blocks of high velocity material. Conjugate faults are also revealed by the seismicity pattern. Similar to the tomographic images of strike-slip faults (previous section) it seems that the extent of the rupture area is limited by material heterogeneities: the upward termination of the main shock rupture coincides with the boundary between Franciscan rocks and the Great Valley sequence (Eberhart-Phillips, 1989). In this case, the comparison of LET results with reflection studies has enhanced the ability of seismic tomography techniques to study the relationship between material properties heterogeneities and the faulting process.

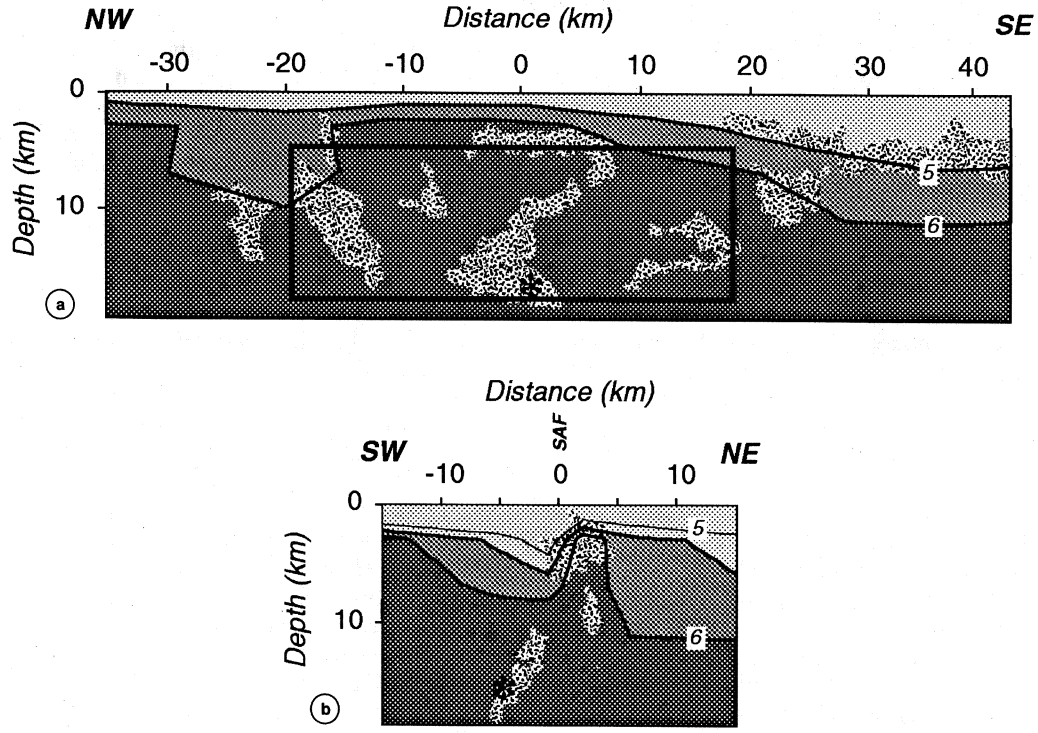


**Fig. 2a,b.** Loma Prieta seismic zone: velocity structure, 1989 main shock location (star), aftershocks, and area of uniform slip distribution according to Lisowski *et al.* (1990). We show two vertical sections, (a) along and (b) across the fault. Symbols as in fig. 1a,b (redrawn after Michael and Eberhart-Phillips, 1991).

The second example of LET studies applied to thrust faults is the Friuli region, Northern Italy, described by Amato *et al.* (1990). In this area two $M = 6.5$ earthquakes occurred in 1976 (May and September) and several thousands of aftershocks were subsequently recorded by a local network. Fault plane solutions of the strongest events revealed thrust faulting on nearly horizontal east-west striking thrust faults. LET results, shown in a north-south vertical cross-section (fig. 4), depict the southward thrust of «alpine» structures over the Friuli platform. A gravity modeling along the N-S profile provides further constraints to the crustal section (Amato *et al.*, 1990). Seismicity is mostly concentrated in the HVZ and in the transitional neighbouring zones. The shape of the velocity anomalies along the N-S profile (fig. 4) suggests the presence of a southward verging structure at a depth of about 5 km, roughly limited by the 6.2 km/s isoline, constituted by a wedge of metamorphic rocks. This structure is thrust southward over the metamorphic basement, which is characterized by higher velocity ($\geq 6.4$ km/s). Most of the earthquakes occur in the volume limited by the 6.2 km/s isoline; the fault planes associated with the strongest events are located at 6-9 km depth at the base of this structure (fig. 4). Thus, the seismogenic structure responsible for the frequent seismicity of the Friuli region is constituted by this high-velocity high-density body.

As pointed out by Stein and King (1984), the reconnaissance of buried seismogenic

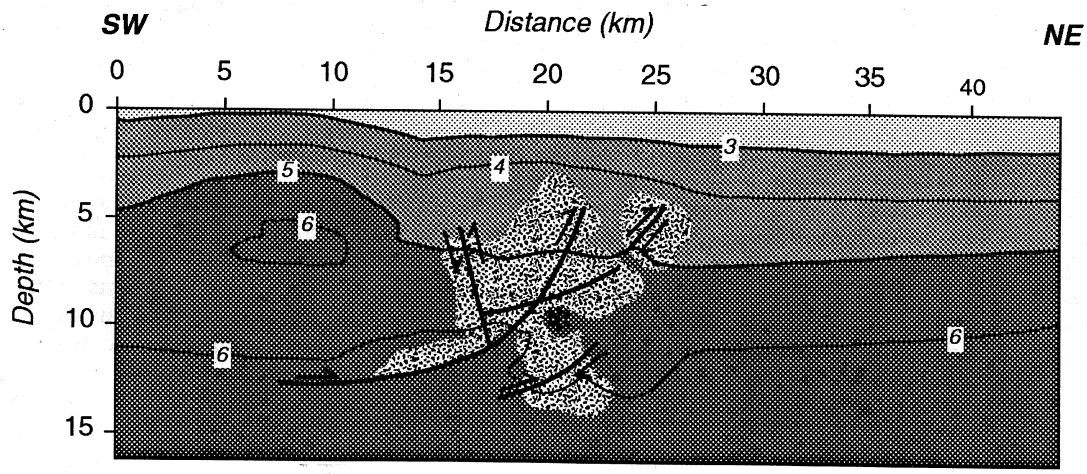


**Fig. 3.** Coalinga: vertical section across the fault showing the three-dimensional velocity structure, aftershock hypocenters, and main active faults (redrawn after Eberhart-Phillips, 1993).

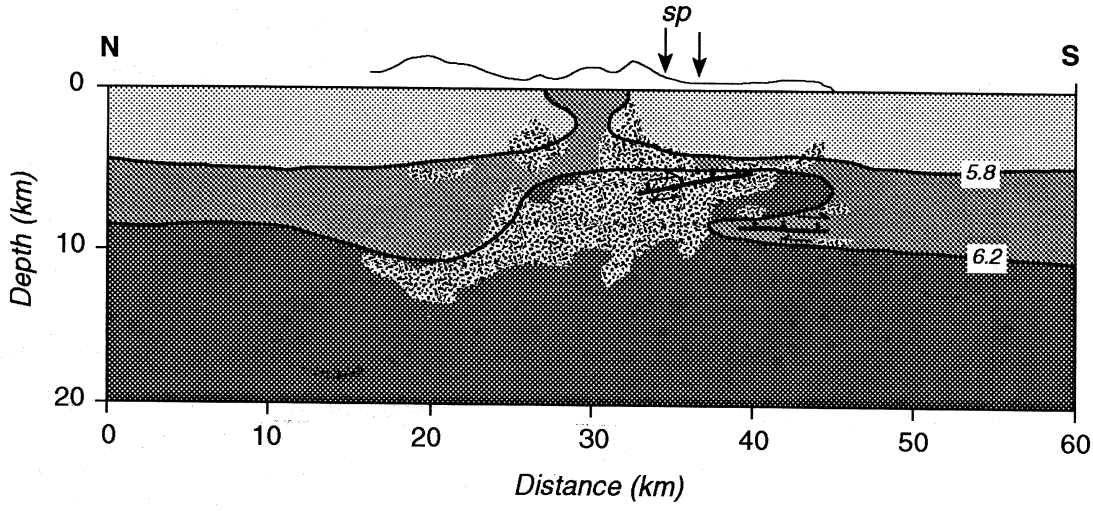


**Fig. 4.** Friuli: velocity structure, aftershocks, and hypothesized thrust faults in a N-S vertical section across the blind seismogenic structure (redrawn after Amato *et al.*, 1990).

structures is extremely important in order to evaluate the seismic potential of active regions, particularly when these structures do not show any surface evidence. In thrust fault regions, LET studies may provide useful information to this goal.

## 4. Irpinia-gate

The 23 November 1980, Irpinia earthquake is one of the largest normal faulting events ($M_S$ = 6.9), where several studies have been carried out (Deschamp and King, 1984; West-

away and Jackson, 1987). A 38 km long, NW-SE surface rupture was mapped by Pantosti and Valensise (1990), and the complex source has been recognized as consisting of three subevents (Bezzeghoud, 1987; Bernard and Zollo, 1989; Giardini, 1990; Cocco and Pacor, 1993). The relation between source dynamics, amount of observed slip, and geologic structures spurred us to further investigate the role of lithological heterogeneities in rupture propagation. Amato *et al.* (1992) demonstrated the efficacy and robustness of the tomographic study, inverting more than 9000 travel times from 612 local earthquakes which occurred between 15 days and 3 months after the mainshock.

### 4.1. *Irpinia: resolution*

The aftershocks are spread in a $60 \times 20 \times 12$ $km^3$ volume (fig. 5). This geometry mitigates resolution artifacts (smearing of anomalies) that affect LET for strike-slip events where most of the rays travel away from a vertical plane (the fault) towards the surface without

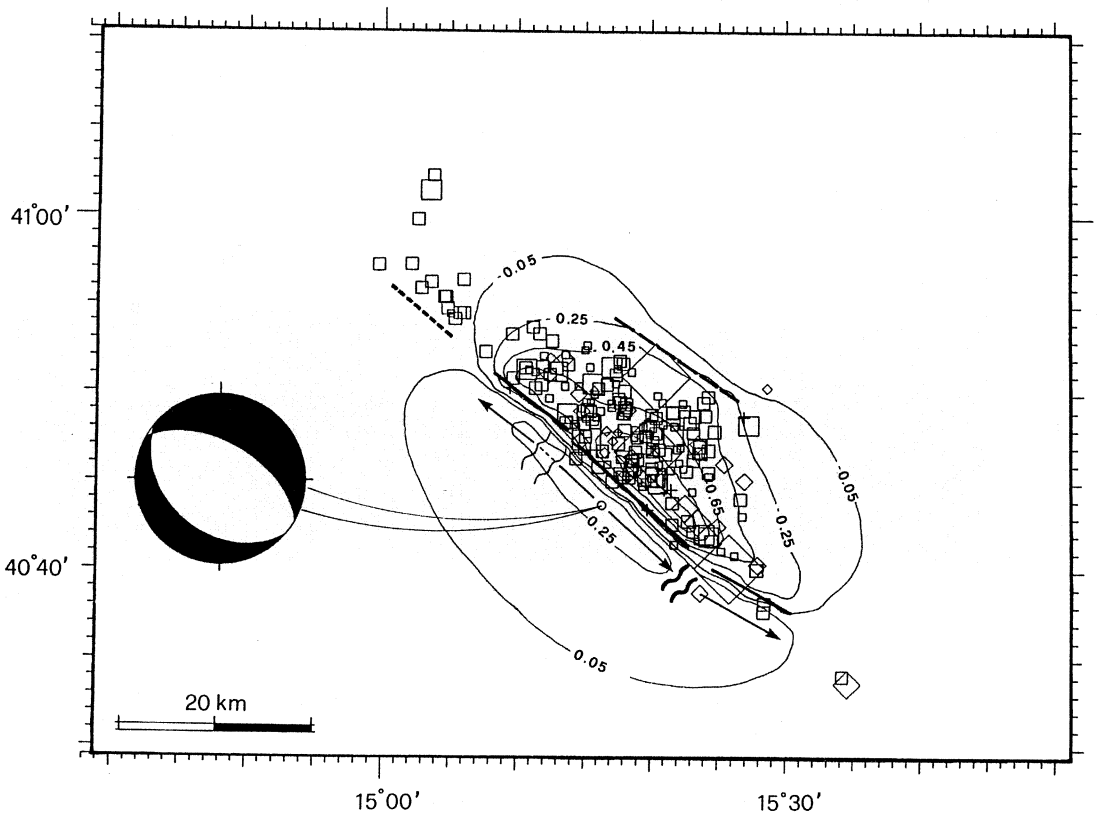


**Fig. 5.** Interpretative synthetic model of the Irpinia earthquake (from Amato *et al.*, 1992). Aftershocks, main shock focal mechanism, and proposed fault segments are plotted (see Cocco and Pacor, 1993, for details). The arrows indicate the direction of the rupture propagation, interrupted by two barriers (≈) (a strong barrier to the southeast, and a «relaxation» barrier to the northwest). The isolines are the elevation changes predicted by the source model proposed by Pantosti and Valensise (1990).

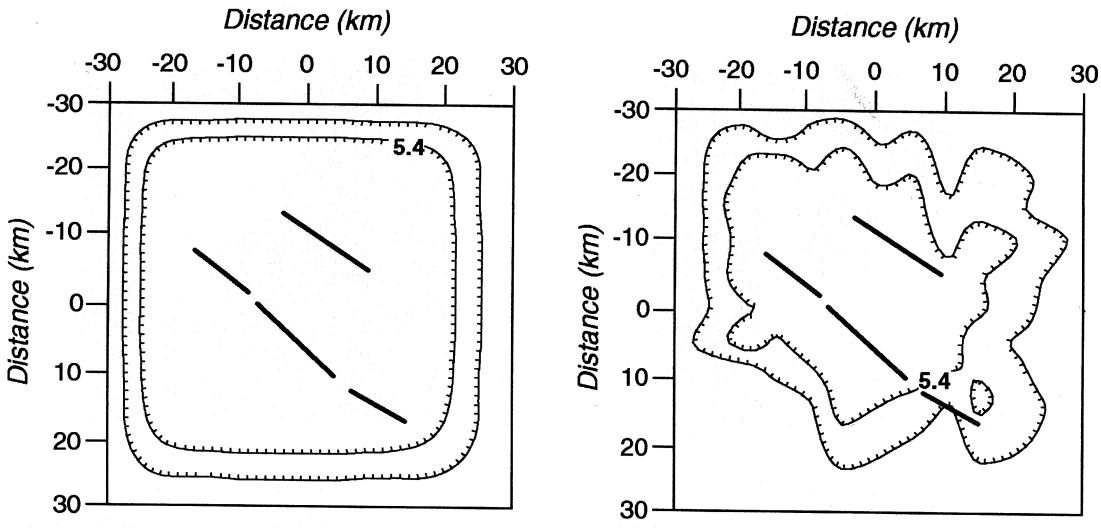


**Fig. 6.** Comparison between the recovered (left) and the synthetic (right) velocity model at the seismogenic depth of 6 km.

criss-crossing. The Irpinia data are homogeneously distributed in space. Data homogeneity is particularly important for inverting local earthquake data. Amato *et al.* (1992) and Malagnini *et al.* (1993) performed a careful analysis of the model resolution and velocity anomalies reliability, individuating a well resolved central volume from 3 to at least 9 km depth.

In several LET studies a relation between earthquakes and high velocity is observed, and we investigate the relation between velocity and hypocentral parameters. We performed a simple synthetic test to evaluate whether the trade off between event location (especially origin time) and velocity structure could result in an artificial velocity increase close to the seismic source. This test was aimed at verifying the reliability of high velocity anomalies often found within the seismogenic zone. Synthetic ray-paths have been traced through a low-velocity region located at seismogenic depths (6-9 km). Then, we inverted the synthetic travel times with a homogeneous starting model, adding random noise to the data. The comparison between synthetic and recovered models (fig. 6) shows that the low velocity anomaly is reproduced at seismogenic depths in the well resolved central volume, and event mislocation does not affect the velocity computation. In the periphery of the model we observe a degradation of the recovered images, suggesting that one should not speculate on velocity anomalies in these regions.

### 4.2. *Irpinia: velocity images*

Figure 7a,b shows the $V_p$ three-dimensional images. In layer 1, at a depth of 3 km, we observe a slight HVZ beneath Mt. Picentini and Mt. Marzano, separated by low velocity in the Sele Valley. The station corrections used in the inversion (see Amato *et al.*, 1992) mitigate the shallow velocity contrasts previously found by Amato and Selvaggi (1990). A second small LVZ is present beneath S. Gregorio, at the southern end of the main fault segment mapped by Pantosti and Valensise (1990). A strong positive anomaly is found at the northern end of the fault segments. In layer 2, at a depth of 6 km, the prominent feature is a sharp

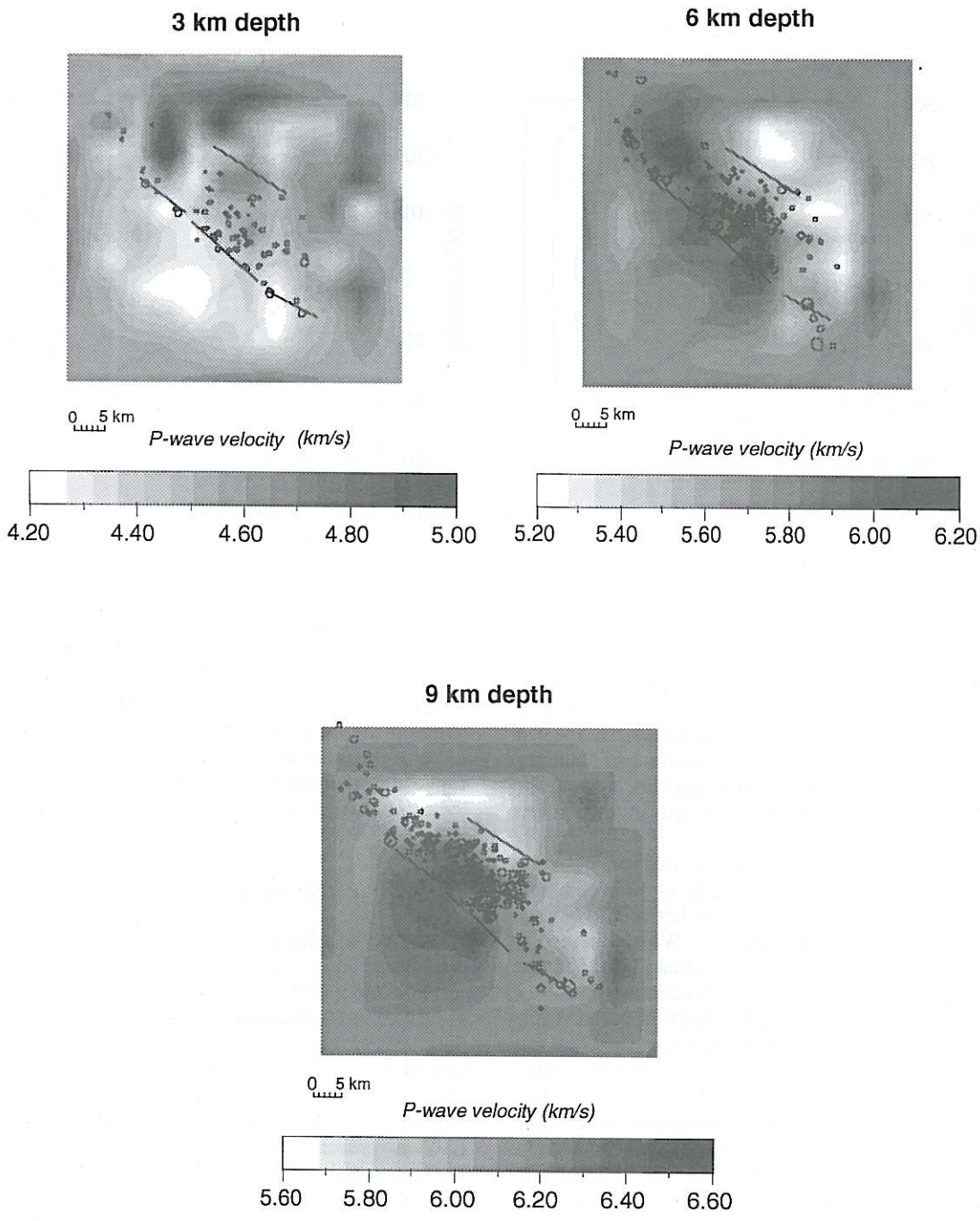


**Fig. 7a.** Velocity tomograms at 3, 6, 9 km depth. Earthquakes occurring within 1 km from each layer are represented. Solid lines indicate the fault traces.

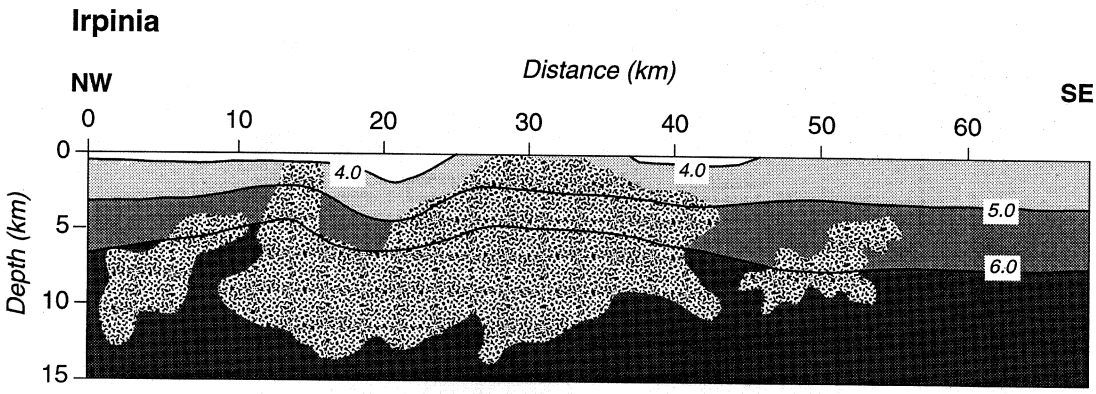


**Fig. 7b.** NW-SE vertical section along the fault (from Amato *et al.*, 1992).

contrast between high velocities in the southwestern region and low velocities in the northeastern area. The HVZ, striking NW-SE, approximately corresponds with the location at depth of the fault that ruptured during the mainshock. In layer 3 (9 km deep) we still find a positive anomaly in the seismogenic region, confined by low velocities in the surrounding. The crustal structure appears more homogeneous than in the shallower layers.

### 4.3. *Irpinia: velocity images and mainshock*

At the depth of the mainshock nucleation (~ 10 km, Westaway and Jackson, 1987), we observe that the seismogenic structure lies within the high velocity. The ruptured area is confined by lower velocities, and is depicted by the extension of the HVZ. We associate high velocity with the presence of high strength rocks that release energy with sudden brittle failure, and are likely to produce large events.

At shallower depth, the structural heterogeneities increase along the fault as shown by tomograms (see fig. 7a,b). This is due to a highly heterogeneous structural setting where several thrust faults and folds developed during the formation of the Apenninic chain. The upper crustal structure here is composed of carbonate units overthrusted on flysch sequences, which are locally collapsed in shallow basins, giving rise to a lithologic puzzle. The relative homogeneity in the deep basement (8-10 km depth) evident in layer 3 is interrupted at shallower depth by the strongly deformed Apenninic units. Thus, the heterogeneous distribution of materials with different frictional properties separates zones where unstable sliding may occur from zones governed by stable sliding. The former, characterized by high velocities, correspond to areas with large coseismic slip on the fault (Cocco and Pacor, 1993), and surface rupture (Pantosti and Valensise, 1990). Conversely, the LVZ at 6 and 3 km depths beneath the Sele Valley and S. Gregorio can be related to weak materials undergoing stable slip. In these two zones a deficit of slip on the fault, no or little surface rupture, and a weak aftershock activity are observed.

### 4.4. *Irpinia: velocity images and aftershocks*

The most obvious pattern is the concentration of aftershocks in the NW-SE HVZ. We observe that almost no earthquakes occur in the LVZ beneath the Sele Valley, or to a lesser extent, beneath S. Gregorio. The stable sliding mechanism invoked for these two regions implies that the rocks here are not able to accumulate stress and release it by brittle failure. These two stable areas are probably examples

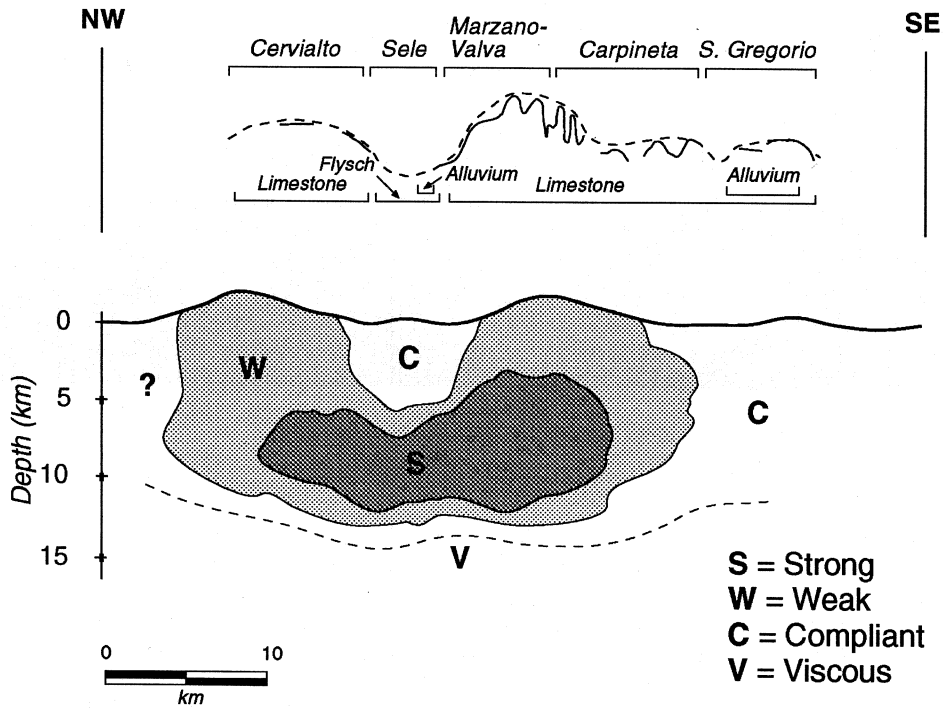


**Fig. 8.** Synthetic sketch of the Irpinia seismogenic zone following the model of Boatwright and Cocco (1994). Three different areas can be identified from velocity tomograms and other seismologic and geologic data, representing rocks with different material properties and then rheologic behavior.

of the compliant behavior of Boatwright and Cocco (1994), whereas the seismogenic zone acts as a strong region, characterized by large coseismic slip during large events, and aftershock clustering. We observe that the largest aftershocks concentrate at the tips of fault segments, where stress concentrations develop after the main rupture due to the heterogeneous distribution of frictional properties along the fault.

Figure 8 is a representation of the Irpinia fault system following the model proposed by Boatwright and Cocco (1994). A strong region (S) characterized by large coseismic slip and aftershocks is predominant at seismogenic depth. In the uppermost crust (0-5 km) large lithologic heterogeneities are evident. Two brittle regions (W) are characterized by aftershocks and rupture propagation through the surface, separated by a zone with stable sliding behavior (C). We hypothesize another compliant (C) region in the southeastern end of the fault zone. At greater depth (more than 12 km) viscous (V) behavior characterizes the ductile lower crust.

## 5. Conclusions

The review of LET studies in several seismic zones together with the example of the Irpinia earthquake reveals the tendency for seismicity to be associated with *high velocity* regions. *High velocities* are the expression of strong fault segments characterized by unstable slip, whereas *low velocities* represent weak rocks with stable slip. Thus, well defined three-dimensional $V_p$ images enable us to iden-

tify zones with different rheologic and seismic characteristics, with the possibility of predicting their behavior. As a future direction, the extension of seismic tomography to $V_p/V_s$ and attenuation studies will greatly improve our knowledge of the deep structures and their relation with earthquake occurrence.

We used the Irpinia earthquake as an example of how to derive fault heterogeneities from tomograms. We suggest that lithologic and structural heterogeneities that developed during the Apenninic deformation are the main factors responsible for variations in the seismogenic behavior at shallow crustal depth. Thus, earthquake generation and propagation is controlled by material property variations along the fault. Along and across the fault, high velocity anomalies indicate regions with unstable behavior, while low velocity zones are presumably indicative of stable slipping areas. At seismogenic depth, the fault segments characterized by high strength are imaged as high velocity features, enabling us to identify the fault patches that are expected to generate large earthquakes.

## Acknowledgements

We thank M. Cocco and J. Boatwright for helpful suggestions, criticism and a continuous encouragement in developing these ideas, D.P. Hill for the review of the manuscript. We are also greatful to D. Riposati for help in drafting the figures.

*REFERENCES*

AKI, K. and W.H.K. LEE (1976): Determination of three dimensional velocity anomalies under a seismic array using first *P* arrival times from local earthquakes 1. A homogeneous initial model, *J. Geophys. Res.*, **81**, 2356-2364.

ALLEN, C.R. (1981): The modern San Andreas fault, in *The geotectonic Development of California*, edited by W.G. ERNST, (Prentice-Hall), 512-534.

AMATO, A. and G. SELVAGGI (1990): Aftershock relocation and crustal structure in the epicentral region, in *Proceedings of the «Irpinia Dieci Anni Dopo» Meeting, Sorrento, Italy, 19-24 November 1990* (Istituto Nazionale di Geofisica, Roma), 34-39.

AMATO, A., R. DE FRANCO and L. MALAGNINI (1990): Local source tomography: applications to Italian areas, *Terra Nova*, **2**, 596-608.

AMATO, A., C. CHIARABBA, L. MALAGNINI and G. SELVAGGI (1992): Three-dimensional *P*-velocity structure in the region of the $M_s$ = 6.9 Irpinia, Italy, normal faulting earthquake, *Phys. Earth Planet. Int.*, **75**, 111-119.

BAKUN, W.H. and T. V. MCEVILLY (1984): Recurrence models and Parkfield, California, earthquakes, *J. Geophys. Res.*, **89**, 3051-3058.

BERNARD, P. and A. ZOLLO (1989): The Irpinia (Italy) 1980 earthquake: detailed analysis of a complex normal fault, *J. Geophys. Res.*, **94**, 1631-1648.

BEROZA, G.C. (1991): Near-source modeling of the Loma Prieta earthquake: evidence for heterogeneous slip and implications for earthquake hazard, *Bull. Seismol. Soc. Am.*, **81**, 1603-1621.

BEZZEGHOUD, M. (1987): Inversion et analyse spectrale des ondes *P*, Thèse de Doctorat, Université de Paris VII.

BOATWRIGHT, J. and M. COCCO (1994): The effect of lateral variations of friction on crustal faulting, *Annali di Geofisica*, **37**, 1391-1413 (this volume).

BYERLEE, J. (1990): Friction, overpressure and fault normal compression, *Geophys. Res. Lett.*, **17**, 2109-2112.

CHESTER, F.M., J.P. EVANS and R.L. BIEGEL (1993): Internal structure and weakening mechanisms of the San Andreas fault, *J. Geophys. Res.*, **98**, 771-786.

COCCO, M. and F. PACOR (1993): The rupture process of the 1980, Irpinia, Italy earthquke from the inversion of strong motion waveforms, *Tectonophysics*, **218**, 157-177

DESCHAMPS, A. and G.C.P. KING (1984): Aftershocks of the Campania-Lucania (Italy) earthquake of 23 November 1980, *Bull. Seismol. Soc. Am.*, **74**, 2483-2517.

DIETZ, L.D. and W.L. ELLSWORTH (1990): The October 17, 1989, Loma Prieta, California, earthquake and its aftershocks: geometry of the sequence from high-resolution locations, *Geophys. Res. Lett.*, **17**, 1417-1420

EBERHART-PHILLIPS, D. (1989): Investigations of crustal structure and active tectonic processes in the Coast Ranges, Central California, Ph.D. Thesis, Standford University, January 1989.

EBERHART-PHILLIPS, D. (1990): Three-dimensional *P* and *S* velocity structure in the Coalinga region, California, *J. Geophys. Res.*, **95**, 15343-15363.

EBERHART-PHILLIPS, D. (1993): Local earthquake tomography: earthquake source region, in *Seismic Tomography: Theory and Practice*, edited by H.M. IYER and K. HIRAHARA (Chapman and Hall, London), 614-643.

EBERHART-PHILLIPS, D. and A.J. MICHAEL (1993): Three-dimensional velocity structure, seismicity, and fault structure in the Parkfield region, Central California, *J. Geophys. Res.*, **98**, 15737-15758.

FOXALL, W., MICHELINI A. and T. V. MCEVILLY (1993): Earthquake travel time tomography of the Southern Santa Cruz Mountains: control of fault heterogeneity of the San Andrea fault zone, *J. Geophys. Res.*, **98**, 17691-17710.

GIARDINI, D. (1990): Teleseismic observation of the November 23, 1980 Irpinia earthquake, in *Proceedings of the «Irpinia Dieci Anni Dopo» Meeting, Sorrento, Italy, 19-24 November 1990* (Istituto Nazionale di Geofisica, Roma), 19-24.

HILL, D.P. (1993): A note on ambient pore pressure, fault

confined pore pressure, and apparent friction, *Bull. Seismol. Soc. Am.*, **83**, 583-586

Lees, J.M. and P.E. Malin (1990): Tomographic images of *P* wave velocity variation at Parkfield, California, *J. Geophys. Res.*, **95**, 21793-21804.

Lisowsky, M., W.H. Prescott, J.C. Savage, *et al.* (1990): Geodetic estimate of coseismic slip during the 1989, Loma Prieta, California, earthquake, *Geophys. Res. Lett.*, **17**, 1437-1440.

Malagnini, L., C. Chiarabba and A. Amato (1993): Reliability of images obtained from local earthquake seismic tomography, EUG Congress, Strasbourg, April 1993 (abstract).

Michael, A.J. and D. Eberhart-Phillips (1991): Relations among fault behavior, subsurface geology, and three-dimensional velocity models, *Science*, **253**, 651-654.

Michelini, A. and T. V. McEvilly (1991): Seismological studies at Parkfield, I, simultaneous inversions for velocity structure and hypocenters using cubic B-splines parameterization, *Bull. Seismol. Soc. Am.*, **81**, 524-552.

Oppenheimer, D.H. (1990): Aftershock slip behavior of the 1989 Loma Prieta, California earthquake, *Geophys. Res. Lett.*, **17**, 1199-1202.

Pantosti, D. and G. Valensise (1990): Faulting mechanism and complexity of the 23 November, 1980, Campania-Lucania earthquake inferred form surface observations, *J. Geophys. Res.*, **95**, 15319-15341.

Pavlis, G.L. and J.R. Booker (1980): The mixed discrete-continuous inverse problem: application to the simultaneous determination of earthquake hypocenters and velocity structure, *J. Geophys. Res.*, **88**, 4801-4810.

Rice, J.R. (1992): Fault stress states, pore pressure distributions, and the weakness of the San Andreas fault, in *Fault Mechanics and Transport Properties in Rocks*, edited by B. Evans and T.F. Wong (Academic, San Diego, Calif), 475-503.

Roecker, S.W. (1993): Tomography in zones of collision: practical considerations and examples, in *Seismic Tomography: Theory and Practice*, edited by H.M. Iyer and K. Hirahara (Chapman and Hall, London), 584-612.

Scholz, C.H. (1990): *The Mechanics of Earthquake and Faulting* (Cambridge University Press, New York).

Schwartz, D.P. and K.J. Coppersmith (1984): Fault behavior and characteristic earthquakes: examples from the Wasatch and San Andreas fault, *J. Geophys. Res.*, **89**, 5681-5698.

Segall, P. and R. Harris (1987): Earthquake deformation cycle on the San Andreas fault near Parkfield, California, *J. Geophys. Res.*, **92**, 10511-10525.

Segall, P. and M. Lisowsky (1990): Surface displacement in the 1906 San Francisco and 1989 Loma Prieta earthquakes, *Science*, **250**, 1241-1244.

Stein, R.S. (1993): Divining blind faults, growing folds, and hidden earthquakes with geodesy, *EOS Trans AGU*, **74**, 59.

Stein, R.S. and G.C.P. King (1984): Seismic potential revealed by surface folding: 1983 Coalinga, California, earthquake, *Science*, **225**, 869-872.

Thurber, C.H. (1983): Earthquake locations and three-dimensional crustal structure in the Coyote Lake area, Central California, *J. Geophys. Res.*, **88**, 8226-8236.

Thurber, C.H. (1992): Hypocenter-velocity structure coupling in local earthquake tomography, *Phys. Earth Planet Int.*, **75**, 55-62.

Thurber, C.H. (1993): Local earthquake seismic tomography: velocities and $V_p/V_s$-theory, in *Seismic Tomography: Theory and Practice*, edited by H.M. Iyer and K. Hirahara (Chapman and Hall, London), 563-583.

Westaway, R. and J. Jackson (1987): The earthquake of 1980 November 23 in Campania-Basilicata (Southern Italy), *Geophys. J. R. Astr. Soc.*, **90**, 375-443.

Zhao, D. and H. Kanamori (1992): *P*-wave image of the crust and uppermost mantle in Southern California, *Geophys. Res. Lett.*, **19**, 2329-2332.